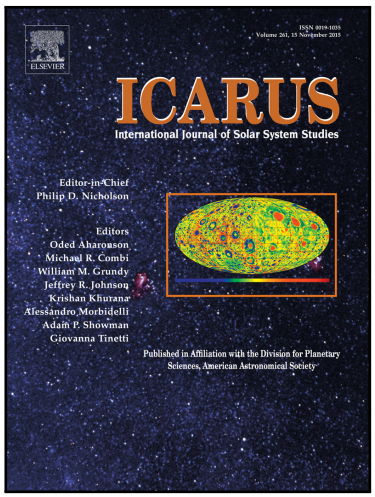

Deconvolution of mixtures with high plagioclase content for the remote interpretation of lunar plagioclase-rich regions

Serventi Giovanna , Carli Cristian , Sgavetti Mariaamaria

PII: S0019-1035(16)00031-2
DOI: 10.1016/j.icarus.2016.01.020
Reference: YICAR 11899

To appear in: *Icarus*

Received date: 6 July 2015
Revised date: 2 November 2015
Accepted date: 3 January 2016

Please cite this article as: Serventi Giovanna , Carli Cristian , Sgavetti Mariaamaria , Deconvolution of mixtures with high plagioclase content for the remote interpretation of lunar plagioclase-rich regions, *Icarus* (2016), doi: 10.1016/j.icarus.2016.01.020

Highlights

- MGM deconvolution of plagioclase-dominated mixtures
- Pyroxene, even if only 1%, is recognizable in mixtures with plagioclase
- Olivine, if less than 5%, can be masked by iron-rich plagioclase
- Terrestrial analogues are useful for the mineralogical interpretation of a planet
- The spectral convergence of spectra can led to misleading interpretations

Deconvolution of mixtures with high plagioclase content for the remote interpretation of lunar plagioclase-rich regions

Authors (Surname; Given name) and affiliations

Serventi Giovanna, Department of Physics and Earth Sciences, University of Parma, Italy giovanna.serventi@unipr.it

Carli Cristian, IAPS-Inaf, Tor Vergata, Roma, Italy cristian.carli@iaps.inaf.it

Sgavetti Maria, Department of Physics and Earth Sciences, University of Parma, Italy maria.sgavetti@unipr.it

Corresponding author

Serventi Giovanna giovanna.serventi@unipr.it

Department of Physics and Earth Sciences, Viale delle Sceinze 157/A, University of Parma, Italy

+39 3494900919

Keywords: Moon, surface, Spectroscopy, Mineralogy

Abstract

Anorthositic rocks are widespread on the lunar surface and have probably been formed by flotation of PL over a magma ocean. A large portion of pristine rocks are characterized by a low Mg/(Mg+Fe) ratio, and have been classified as ferroan anorthosite, and recently, after observation from SELENE Spectral Profiler,pure anorthosites regions with more than 98% PL have been recognized.

In this paper we analyze a set of mixtures with PL content similar to the ferroan anorthosites and to the pure anorthosite regions, using the Origin Software and the Modified Gaussian Model.We consider three plagioclases with varying FeOwt% contents (PL1, PL2 and PL3)andthree mafic end-members (1)100% orthopyroxene, (2) 56% orthopyroxene and 44% clinopyroxene, and (3) 100% olivine (OL). The spectral parameters considered here are: band depth, band center, band width, c0 (the continuum intercept) and c1 (the continuum offset).

Here we have shown that in pyroxene (PX)-bearing mixtures, the PX is distinguishable even in mixtures with only 1% PX and that PX band at ca. 900 nm is always deeper than PL1 band while PL2 and PL3are deeperthan OPX 900 nm band from95, 96% PL. In OL-bearing mixtures, OL detection limit is 2% when mixed with PL1, and 3% and 4% if mixed with PL2 and PL3.

We also demonstrated how spectral parameters vary with PL%, and, generally, increasing the PL content: (1) 1250 nm band depth decreases when mixed with OL, while it deepens in mixtures with PX; (2) 1250 nm band centers generally move towards longer wavelength for PL1-bearing mixtures, while do not show significant variationsconsidering PL2/PL3-mixtures; (3)1250 nm band width of PL1 in E1 and E5-mixtures substantially widens while in other mixtures itonly slightly varies.

Here we also proposed an application to a real case, from Proclus crater, revealing how studying terrestrial analogues is fundamental to infer hypothesis on the mineralogical composition of a planetary surface, but also how the spectral convergence of spectra characterized by different compositions can led to misleading interpretations.

1. Introduction

The Moon is one of the most studied planetary bodies across the Solar System. Its crust is composed with a very large anorthositic complex (Warren, 1895) and the plagioclase (PL) is widespread on the surface, both in Maria and in Highland regions (Hiesenger and Head, 2006 and references therein). Lunar meteorites, returned samples and remote sensed data, both Earth-based and from orbit, permitted the analysis of the lunar surface mineralogical composition. In particular, several missions spectroscopically measured the lunar surface, e.g. Clementine (McEwen and Pieters, 1997), Kaguya/SELENE (Kato et al., 2008; Ohtake et al., 2008) and Chandrayaan-1 (Pieters et al., 2009; Boardman et al., 2011; Green et al., 2011).

Studying the Apollo samples, it has been observed that a large portion of pristine rocks were characterized by a low Mg/ (Mg+Fe) ratio (Warren, 1985), thus differing from the Mg-rich rocks, and so classified as ferroan anorthosite (FAN). The authors also stated that the mean PL content in FAN is 90-92%, with low content of ferroan mafic minerals (see also McGee, 1993), e.g., orthopyroxene (OPX), clinopyroxene (CPX) and olivine (OL). FAN rocks have probably been formed by flotation of PL over a magma ocean, and Mg-rich magmas intruded the anorthositic crust thus forming the Mg-suite (Smith et al., 1970; Wood et al., 1970; Warren, 1985; Brown and Elkins-Tanton, 2009).

Tompkins and Pieters (1999) show the spectral data acquired by the UVVIS camera (0.4-1.0 μm), onboard Clementine mission, from 109 impact craters with central peaks or peak rings. It is widely

acknowledged that original material, not affected by the space weathering, have been uplifted to the surface in central peaks and in peak rings: so, their composition and mineralogy are expected to reflect deeper crustal compositions. The presence of PL has been inferred from the presence of weak or absent mafic absorption bands (calculated from the 1000 nm band depth) and from the spectral curvature of the 1000 nm band (i.e., the angle formed between 750, 900 and 950 nm). In general, Tompkins and Pieters (1999) concluded that the lunar crust is extremely anorthositic, with a PL content ~82%.

In some cases, featureless spectra, such as full-resolution telescopic data from the Orientale Basin, were related to shocked PL (Spudis et al., 1984), because high shock pressure weakens the PL absorption band (Adams et al., 1979).

Early investigations based on Earth-based telescopic data (Spudis et al., 1984; Bussey and Spudis, 2000; Hawke et al., 2003) revealed featureless high albedo material inferred to be associated with shocked anorthosites.

In 2007, the Japanese SELENE spacecraft has been launched, carrying onboard the Spectral Profiler (SP), a visible near-infrared (VNIR, 0.5-2.6 μm) spectrometer with a high spectral resolution of 6-8 nm. The spectrometer detected the presence of an absorption band at ca. 1250-1300 nm, consistent with Fe^{2+} transition in crystalline PL, in central peaks of impact craters (Matsunaga et al., 2008). Matsunaga et al. (2008) proposed a new interpretation of Tsiolkovsky central peak, previously classified as OL-rich, as composed with PL and Pyroxene (PX). Ohtake et al. (2009) defined the pure anorthosites (PAN) as regions with more than 98% PL: PAN regions are characterized by a lower limit of PL higher than FAN, thus leading to new constraints on models of the lunar magma ocean evolution. PAN regions have been identified in Tycho, Tsiolkovsky, Orientale, and Jackson craters (Ohtake et al., 2009). Furthermore, Ogawa et al. (2011) detected spectra of high-Ca PX and PL widely distributed in and around the bright-rayed craters, and Yamamoto et al. (2012) showed the presence of both PL and OL in the Copernicus crater.

Recently, the Indian Chandrayaan-1 mission, with the M^3 (Moon Mineralogy Mapper) imaging spectrometer onboard, analyzed the lunar surface with a very high spectral resolution (spectral range: 405-3000 nm; spectral resolution: 10 nm). Basing on M^3 results, Cheek at al. (2012; 2013) confirmed the presence of PAN in the Orientale Basin and in Tsiolkovsky crater, and Kramer et al. (2013) recognized PAN, OPX and OL in Schrödinger Basin.

FAN and PAN rocks, composed with PL content >90% and minor amounts of mafic minerals, were probably formed by the crystallization and segregation of PL inside a magma ocean of the Moon, and the remaining liquid may have produced mafic-rich anorthosite.

2. State of the art

PL, OPX, CPX, and OL have been clearly recognized on the lunar surface (see Papike et al., 1991).

PX are characterized by two absorption bands at ca. 900 nm and ca. 1800 nm (Burns, 1993; Sunshine and Pieters, 1993), due to the Fe^{2+} transition in the M2 site, that shift towards longer wavelengths with increasing Fe^{2+} and Ca^{2+} in the PX crystal structure. Fe^{2+} can enter in the M1 site thus producing an absorption band at ca. 1200 nm (Klima et al., 2008).

OL shows a broad absorption band resolvable with three absorptions at ca. 900, 1050 and 1200 nm, due to Fe^{2+} transition in M1 and M2 sites (Burns, 1993; Sunshine and Pieters, 1998).

PL contains only low amount of Fe^{2+} but an absorption band can be easily recognized at ca. 1250 nm, attributed to Fe^{2+} transition in the large 8-12 fold Ca^{2+} site (Bell and Mao, 1972; Adams and Goulland, 1978; Cheek et al., 2011; 2014; Serventi et al., 2013; 2015).

Although in the literature many works characterizing reflectance spectra of PX, OL and their mixtures can be found (e.g., Cloutis and Gaffey, 1991; Sunshine and Pieters, 1993; 1998; Clenet et al., 2011), PL and mixtures with mafic materials have been poorly analyzed, probably because PL has always been considered a spectroscopically transparent mineral, being, from a stoichiometric point of view, an iron free mineral. The recent identification of a well-defined absorption band at 1250 nm on the lunar surface, interpreted as indicative of the presence of

crystalline PL, makes it fundamental to analyze in detail the spectral behavior of very high PL concentrations in the soils. As previously stated, PL absorption band has been interpreted as the transition of Fe^{2+} in PL crystal structure (Adams and McCord, 1971; Bell and Mao, 1972; Adams and Goulland, 1978). In particular, Adams and Goulland (1978) tried to relate the PL band center to the anorthite (An) content (Ca content). Recently, Cheek et al. (2011) investigated PLs with different iron content, focusing on their spectral behavior. Furthermore, Cheek and Pieters (2014) analyzed PL-rich mixtures with varying content and composition of OL, PX and very high-Mg spinels and demonstrated that PL can significantly contribute to reflectance spectra if strongly absorbing minerals are present in low abundances, particularly in mixtures with PX. In their paper, a PL and six non-PL end-members (one forsteritic OL, one intermediate OL, a OPX, a diopside and two Mg-spinels) have been selected at the 45-75 µm particle size. Non-PL minerals have been mixed with PL in different proportion: in PL dominated mixtures, non-PL minerals vary from 2%, 5%, 7% to 10% , while in non-PL dominated mixtures, non-PL minerals vary from 15%, 20% to 50%. The authors conclude that: 1) 2% OPX is distinguishable from PL, while diopside minimum content is 5%; 2) OL is distinguishable from 5%; 3) mixtures with OL<5% and diopside<5% may be indistinguishable; 3) in mixtures with spinels, the detection of PL depends on the iron content in spinel: iron-rich spinel significantly subdue PL absorption; and 4) PL is recognized in mixtures with spinels more than 15%, while PL results in only a spectrum flattening in mixtures with OPX>10% and in a broadening of the 1000 nm band in mixtures with OL>10%.

Serventi et al. (2013; 2015) analyzed a set of mixtures composed of PL and mafic minerals (a mixture of OPX and CPX, an OPX, an OL and two mixtures with different relative content of OPX and OL), with PL ranging between 20-90%, at two particle sizes, 63-125 and 125-250 µm. The authors shown that, generally, adding PL produces spectra with higher reflectance and reduced spectral contrast. The Modified Gaussian Model (MGM, Sunshine et al., 1990) results also shown that increasing the vol. FeO% in PL, the 1250 nm band deepens in PX-bearing mixtures while it decreases in OL-bearing mixtures, and that the 1250 nm band center always shifts toward longer

wavelengths. The authors also demonstrated how high content of iron-rich PL can play an important role and spectrally dominate when mixed with mafic minerals.

For this reason, it is fundamental to analyze mixtures with PL content >90%, not analyzed in the cited papers, because these concentrations seem to form the lunar highlands.

In this paper, we report analyses of mixtures with PL content similar to FAN and PAN rocks, in order to show the effects of PL on reflectance spectra when >90% of PL, with increasing Fe^{2+}, are mixed with <10% of different mafic minerals. The purposes of our study are to show if it is possible to 1) recognize the PL 98% concentration, stated as the limit for PAN by Ohtake et al. (2009), for different mafic mineral content, thus also involving the mafic mineral's detection limit, as well as 2) discriminate between FAN and PAN. The paper also evaluates different methods for the analysis of spectral parameters as band depth, center and width, such as ORIGIN® and MGM. As in Serventi et al. (2013, 2015), PL with increasing iron content have been chosen, following the suggestion from Taylor et al. (2009). The authors demonstrated how, on the Moon, can crystallize PL with more FeO than the predicted 0.1wt.% (for further details, see Serventi et al., 2013).

In this work, spectral parameter variations are plotted vs. the PL content in the mixtures. This choice, different from the vol. FeO% in PL considered in Serventi et al., 2013; 2015, is because, here, we do not want to explain the PL behavior with increasing FeO content, but we want to investigate the detection limit under which mafic minerals are not detectable, and, if it is possible, to distinguish between FAN and PAN.

3. Analytical approach

A set of three mafic end-members (E1, E4 and E5) and three PL (PL1, PL2 and PL3), already analyzed for 20-90% PL mixtures in Serventi et al. (2013; 2015), was used to produce a total of new 63 mixtures with PL ranging between 90-99%. The mafic end-members are: 1) E1, 44% CPX and 56% OPX mixture; 2) E4, 100% OL; and 3) E5, 100% OPX. The PLs, PL1, PL2 and PL3, have a Fe^{2+} content increasing from 0.1, 0.36 to 0.5 wt.%, respectively; PL1 (An_{45}) is a more sodic PL than

PL2 and PL3 (An_{80}). Adams and Goulland (1978) analyzed PL with different An content but also with a variable iron content. The authors shown that the PL with the position at the highest wavelength is PL with An_{65}; however, it is also clear that the An_{65} is also the sample with the highest iron content. Comparing their figs. 2 ,3 a correlation between position and iron content seems to be reasonable, whereas it is not clear if the band position shifting is related to the An content, as suggested. For this reason, in this work, even if we are dealing with a PL (PL1) characterized by a different An content, we plot our results versus the iron content, neglecting the Na/Ca ratio, because the PL Crystal Field absorption bands are due to iron transitions in mineral crystal lattice (Burns, 1993).

The PL content ranges between 90 and 99 wt.%, and consequently the mafic content from 10 to 1 wt.%. Mixtures were prepared at a fine particle size, 36-63 μm, more suited for the lunar soil size (Papike et al., 1991) than the sizes analyzed in Serventi et al. (2013; 2015). Tab. 1 shows the chemistry, the FeO wt.% content, as well as the geological setting of each end-member.

Spectra of each mixture were acquired at room temperature and normal atmospheric pressure with a Field-Pro Spectrometer mounted on a goniometer (Istituto di Astrofisica e Planetologie Spaziali, Inaf-IAPS, Roma). The spectra were acquired with a spectral resolution of ~3 nm in the VIS and of ~10-12nm in the NIR, with $i=30°$ and $e=0°$. The source used was a QTH (Quartz Tungsten Halogen) lamp and the spot illuminated has an area of ca. 0.5cm^2. The calibration of the spectrometer was performed with Spectralon® optical standard (registered trademark of Labsphere, Inc.). Reflectance spectra and continuum-removed spectra are shown in Fig. 1 and 2, respectively. Spectra were first analyzed using ORIGIN® software, and were then deconvolved applying the MGM algorithm (Sunshine et al, 1990).

4. Overall spectral shape variations

The effects of mixture variations on the spectral shape were first analyzed considering reflectance spectra and continuum removed spectra (Fig. 2), using the software ORIGIN® and considering the

continuum line, function of wavelength, as the straight-line segments that join the reflectance maxima in the spectrum (Clark and Roush, 1984). Figs. 1 and 2 show that, generally:

1) increasing the PL content in mixtures, spectra have reduced spectral contrast and high albedo (Fig. 1,2);
2) in PX-bearing mixtures, the PX band I at ca. 900-1000 nm is detectable even in mixtures with only 1% PX (Fig. 2a-f), though in mixtures composed with PL3 and E1 the absorption band I is just a flattening (Fig. 2f);
3) in mixtures with PL1 and PX-bearing end-members, PX band I is always deeper than PL band and PX band II is deeper than PL till 98% PL (Fig. 2a,d);
4) in mixtures with iron-richer PL, PL2 dominates from 96% PL and PL3 from 95% PL (Fig. 2b,c and e,f). In E1-mixtures PL is deeper than PL in E5-mixtures;
5) OL is characterized by three absorptions, at ca. 900, 1050 and 1200 nm (Burns, 1993; Sunshine and Pieters, 1998) due to the transition of Fe^{2+} in the M1 and M2 sites of olivine. PL absorbs at ca. 1250 nm (Adams and Goulland, 1978). OL band 3 and PL band occur in a very narrow spectral range and the PL absorption is clearly superimposed on the OL band 3, so that it cannot be discriminated from the OL absorption assigned to Fe^{2+} in M1. Consequently, we consider OL band 3 and PL absorption as a unique composite (COMP) band, whose spectral parameters give information about the PL content;
6) in OL-mixtures, when mixed with PL1, OL is clearly recognizable till 98% PL (Fig. 2g), while, if mixed with PL2 and PL3 (Fig. 2h,i), it is masked from 97% and 96% PL, respectively; and
7) in mixtures with OL and PL2/PL3 (Fig. 2h,i), in the 1500-2000 nm spectral region a clear decreasing in the reflectance is visible, even if no absorption bands are expected in this PX-free spectra. This can be probably related to the iron-rich composition of PL, as shown in Hiroi et al. (2012) and in Serventi et al. (2015).

5. Quantitative spectral analyses: MGM deconvolution

5.1 Continuum and Gaussians

For the continuum choice and the Gaussian assignation we followed the procedure described in Serventi et al. (2015). In particular, we considered a fixed continuum tangent to the spectrum reflectance maxima, considered more reliable in the description of the spectrum shape and for modeling the strength of the absorption bands. Continuum is described by two parameters, c0 and c1, in a logarithmic scale of reflectance and function of wavenumber. c0 is the intercept (that is the reflectance value of the spectrum), and c1is the offset. While c0 is always negative, c1 changes from negative to positive values: a negative c1 corresponds to a red slope, while a positive c1 to a blue slope.

We first deconvolved the end-members, mafic and plagioclases, as mineralogically unknown end-members, assigning Gaussians only where either an absorption band or a band asymmetry are visually perceptible (e.g., 900 nm band in E1 is asymmetric towards the NIR region). Then, we deconvolved the mixtures, considering that:

1) the band center and width of mafic minerals depend only on the chemistry (Burns, 1993);
2) the band depth is related to the abundance of a mineral (Sunshine and Pieters, 1993; 1998);
3) PL spectral parameters vary with FeO vol. content in PL (Serventi et al., 2013; 2015);
4) in mixtures composed with OL and PL we cannot assume that the COMP band center and width will remain fixed varying the OL and PL modal abundance.

So, the spectral parameters (band center and band width) assigned to the mafic absorption bands are fixed, whereas the mafic band depth and Gaussians assigned to the 1250 nm absorption band, were left free. Consequently, only the spectral parameters variations of the 1250 nm absorption band and the mafic mineral band depth are here discussed.

In this paper, the ~900 nm and the ~1800 nm PX absorption bands are defined as Band I and Band II, respectively; the OL absorptions are defined Band 1,2 and 3; the composite absorption of PL and

OL band 3 in the 1200 nm region is called COMP Band; and the 1250 nm absorption band is called PL band. A number has been assigned to each Gaussian, as described in Tab.2.

5.2 End-members

Fig. 3 shows the deconvolution of mafic and PL end-members and Tab. 3 and 4 show the spectral parameter values. For the PX-bearing end-members, a Gaussian centered at ca. 840 nm, G5, has been added. Sunshine and Pieters (1993) added a Gaussian in this spectral region for PX mixtures at a coarse particle size; even if in this paper the analyzed particle size is finer then those in Sunshine and Pieters (1993), and in Serventi et al. (2013; 2015), the residual pattern in error after MGM deconvolution with only one Gaussian for the 900 nm band suggested us to add an additional Gaussian, called G5.

As explained in Serventi et al. (2015) and considering that: 1) MGM is never a perfect representation of the Crystal Field absorptions; 2) several factors, e.g. compositional variation, exsolution lamellae or zoning crystals, contribute to electronic absorptions; 3) PX are solid solutions, with high compositional variation within different cations; and 4) Fe^{2+} can enter also in M1 site, influencing the absorption around 1000 nm, G5 has been interpreted as a Gaussian that adjusts the absorption band shape and is not assigned to a particular crystal field transition; for this reason, G5 is not considered in the following discussions.

In particular:

1) E5 is deconvolved with 2 Gaussians: G1 at 930 nm assigned to Fe^{2+} in M2 OPX site and G3 at 1843 nm due to Fe^{2+} transition in OPX M2 site (Fig. 3a);
2) E1 is deconvolved with 4 Gaussians: G1 occurring at 924 nm assigned to Fe^{2+} in OPX M2 site; G2 at 1010 nm assigned to Fe^{2+} in CPX M2 site; G3 at 1851 nm due to Fe^{2+} transition in OPX M2 site and G4 at 2317 nm due to Fe^{2+} transition in CPX M2 site (Fig. 3b);
3) E4 is deconvolved with 3 Gaussians, including G6 at 848 nm and G8 at 1199 nm due to Fe^{2+} transition in OL M1 site, and G7 at 1032 nm due to Fe^{2+} transition in OL M2 site (Fig. 3c);

4) PL1, PL2 and PL3 have been deconvolved with 2 main Gaussians, G10 centered in the 1250 nm spectral region (1271 nm, 1279 nm and 1293 nm, respectively) due to the Fe^{2+} transition in PL crystal structure, and G11 centered in the 1600-1800 nm region (1719 nm, 1675 nm and 1785 nm, respectively) to explain the reflectance decrease in the region as an asymmetry of the PL band (Fig. 3d-f). This band has already been recognized by Pieters et al. (1996), Hiroi et al. (2012) and Serventi et al. (2015) but has not been yet related to any particular crystal field transition;
5) the residuals in PL2 and PL3 deconvolution show a pattern in the 1000-1500 nm spectral region that could indicate the lacking of a Gaussian, but we did not add further Gaussians because no other phases are present. We preferred to explain this behavior with a possible asymmetry or saturation effects of the PL band, also considering the reflectance decrease in the 1600-1800 nm spectral region (see also Serventi et al., 2015).

Comparing with the end-member deconvolution at coarse particle size (Serventi et al., 2015), absorption bands at 36-63 μm are shallower and shifted of only few nanometers with respect to absorption bands at 63-125 μm, shift that falls in the instrumental error of the instrument setup, thus revealing that a finer particle size (36-63 μm) influence the band depth but not the band center.

5.3 Mixtures

As explained in section 5.1, the band center and band width of the mafic end-member Gaussians have been kept fixed in the mixture MGM deconvolution, since band center and band width do not vary with mineral modal abundances (Sunshine and Pieters, 1993; 1998). On the contrary, band depth depends on the modal abundance (Sunshine and Pieters, 1993; 1998), while PL depth, center and width vary with PL modal abundances (Serventi et al., 2015). For this reason mafic band depth and PL spectral parameters vary.

5.3.1 E5+PL

E5 is the OPX (En_{45}-Wo_{46}) endmember. Fig. 4 and 5 show that, adding PL % content:

1) c0 and c1 become less negative. c0 is less negative from PL3, to PL1, while c1 has an opposite behavior and is less negative from PL1 to PL3 (Fig. 4a, b);
2) PL band always deepens (Fig. 4c), while mafic band depth decreases (Fig.5a). Furthermore, PL2 is slightly deeper than PL3, even if PL3 is iron richer than PL2 (Fig. 4c);
3) For PL1, PL2<98% and PL3< 96%, OPX band I (green symbols in Fig. 5a1-a3) is deeper than OPX Band II, while for PL2≥ 98% and PL3≥ 96% there is an overturn and the OPX band II (grey symbols in Fig. 5a1-a3) become deeper (see squares in Fig. 5a1-a3). This behavior is unexpected, and can be related to the presence of PL;
4) PL center does not show significant variations (Fig. 4d) even if 98% and 99% PL3 are shifted towards longer wavelengths with respect to the other PL3-bearing mixtures; and
5) PL band width is almost unchanged in PL2 and PL3 mixtures, while it widens in PL1-mixtures increasing the PL abundance in mixtures (Fig. 4e).

Fig. 4c also shows that the PL depth is very different from 0.1 to 0.36 wt.% FeO PL, while it only slightly varies from 0.36 to 0.5 wt. FeO; PL1 band dominates only for more than 99% PL, while Pl2 and PL3 bands are the deepest from 95% PL (Fig. 5a). Furthermore, the band width shows that the major difference is between PL1 and Pl2, while there is an overlap between PL2 and PL3 (Fig. 4e). c0, c1 and band center are the spectral parameters useful to distinguish PL2 from PL3.

5.3.2 E1+PL

E1 is a mixture of OPX and CPX; the spectral parameter variations are similar to the previous mixtures, but some consideration must be added:

1) The continuum parameters, c0 and c1, have less negative values than E5-mixtures (Fig. 6a,b) and, differently from previous mixtures, c1 in PL2-mixtures is less negative than in PL3-mixtures;

2) PL1 is deeper than CPX from 97% PL and deeper than OPX from 99% PL; PL2 and PL3 dominates from 92% PL (Fig. 7a);
3) The depth overturn between OPX band I and Band II occurs for PL2> 97% and PL3>92% (see squares in Fig. 7a1- a3);
4) PL band center (Fig. 6d) and PL width, with the exception of PL1-mixtures (Fig. 6e), are almost unvaried.

In these mixtures some behaviors already explained in the previous section are emphasized. In particular, Fig. 6c,e show very similar depth for PL2 and PL3 (PL≥ 95%) and a total overlap between PL2 and PL3 width, while Fig. 6d displays how PL1 and PL2 center are very similar. Furthermore, the OPX overturn between Band I and Band II occurs at lower PL % than in E5-mixtures (Fig. 7a).

5.3.3 E4+PL

These mixtures include the OL end-member; in spite of considering, as in previous sections, the PL absorption band, we analyze the COMP band due to the overlapping OL band 3and PL in the 1200 nm spectral region (see point 5 in Section4.).

In particular, with increasing PL content:

1) The continuum parameter c0 is almost unaffected, while c1 becomes less negative (Fig. 8a,b);
2) COMP band becomes less deep but is always deeper than OL band 1 and 2 (Fig. 8c); a 1250 nm band deeper than the PL end-member means the presence of OL, even if not visible in the spectrum. PL2 COMP band is deeper than PL3;
3) COMP band center (Fig. 8d) shifts towards the longer wavelengths; and
4) COMP band width is slightly narrow (Fig. 8e).

Differently from the previous mixtures, 1250 nm band depth becomes less intense and band width narrower; this is related to the presence of OL, that iron richer than PL, spectroscopically dominates

the COMP band. This differs from Serventi et al. (2015) where we have demonstrated how, considering coarse particle sizes, the COMP band becomes less intense till a vol. FeO% value, after which the COMP band deepens.

As previously explained in section 5.2, E4 does not contain PX: for this reason no absorptions are expected in the 1800 nm spectral region. Nevertheless, spectra show a reflectance decrease in that region. In order to describe it, a Gaussian has been added with free spectral parameters, called the 1800 nm Gaussian. Fig. 8f,g and h, show that increasing the PL content in mixtures, the 1800 nm Gaussian deepens, as the 1250 nm band assigned to the PL absorption (see Fig. 4c, 6c), and widens. Also, depth and width increase with increasing FeO content in PL. On the contrary, the 1800 nm band moves towards shorter wavelength, with the exception of 99% PL3 and 100% PL3.

6. Discussions

Here we have shown that in PX-bearing mixtures, the PX is distinguishable even in mixtures with only 1% PX and that PX band I is always deeper than PL1 band while PL2 and PL3 are deeper than OPX band I from 95, 96% PL, respectively. We have also shown that OL detection limit is 2% when mixed with PL1, and 3% and 4% if mixed with PL2 and PL3, respectively.

We also demonstrated how spectral parameters, extrapolated from MGM application, vary with PL% and PL chemistry. However, these variations resulted to be also related to the mafic endmember.

In fact, 1) COMP band depth decreases in OL-bearing mixtures; 2) PL band deepens when PL is mixed with PX; 3) PL band is deeper in E5 OPX-bearing mixtures with respect to OPX-CPX-bearing E1 mixtures; and 4) PL2 band is slightly deeper than PL3 band, even if iron-richer PL are expected to be deeper than iron-poor PL (Cheek et al., 2011). We interpret this behavior as probably due to an effect of saturation in FeO-rich PL3 (Fig. 9a), as also indicated by the presence of a strong 1800 nm band. It can also be related to a different distribution between Fe^{2+}/Fe^{3+}, even if PL2 and PL3 belong to the same intrusive cumulitic layer deposit (Tab. 1). We have also demonstrated how

COMP band depth is particle-size dependent: COMP band decreases in mixtures analyzed in this paper, while it deepens in coarse mixtures with high-PL content, because PL at coarse sizes is deeper than PL at fine sizes (Serventi et al., 2015).

Regarding the band center positions, Fig. 9b shows that increasing PL modal abundances PL band centers generally move towards longer wavelengths for PL1-bearing mixtures, while considering PL2/PL3-mixtures band centers do not show significant variations. In PL-OL mixture, COMP band is centered at shorter wavelength (blue circles in Fig. 9b) with respect to the PL band center in PX-bearing mixtures, as an effect of the presence of OL; the difference is reduced from 90% PL to 99% PL.

More specifically, in PX-mixtures:

1) in PL1-bearing mixtures, OPX+CPX-mixture band centers are at longer wavelengths than OPX-mixtures (light green and pink diamonds in Fig. 9b);
2) in PL2-bearing mixtures, OPX+CPX-mixture and OPX-mixture band centers are at similar wavelength (green and fuchsia empty diamonds in Fig. 9b); and
3) in PL3-bearing mixtures, OPX-mixture band centers are at longer wavelengths than OPX+CPX-mixtures (dark green and violet diamonds in Fig. 9b).

Fig. 9c displays that increasing the PL content PL band width only slightly varies, with the exception of PL1 in E1 and E5-mixtures where PL band substantially widens. Differently from Serventi et al. (2015), here we have shown how PL center and width is almost fixed if we consider mixtures with high iron-rich PL content, where PL becomes a dominant phase.

In any cases all the spectral parameters for the PL converge to the considered PL end-member spectral parameters (grey and black diamonds in Fig. 9).

Another interesting point is that OPX band I and II depth show an inversion in E5 and E1-mixtures. This behavior is more evident in E1-mixtures than in E5-mixtures and in PL3 than in PL1-bearing mixtures, probably related to the 1800 nm PL absorption band (see Figs. 5d1-d3 and 6d1-d3).

In fact, we have shown how OL-mixtures have an absorption in the 1800 nm range, even if not expected from the mafic end-member mineralogy: this can be due to the FeO content in PL. Even if this band has been recognized in the literature (Pieters, 1996; Hiroi et al., 2012; Serventi et al., 2015), it is still unassigned, so future works about synthetic iron-bearing PL will be necessary to investigate this behavior. In this work we have however pointed out a possible correlation of the 1800 nm Gaussian with the FeO content in the PL (see Fig. 8d,f,h).

Furthermore, as already demonstrated in Serventi et al. (2013; 2015), we have shown how PL2 band is deeper than PL3 even if PL2 is iron-poorer than PL3 (see fuchsia and violet diamonds in Figs. 4c, 6c and 8c). This can be probably related to saturation effects that occur in the PL crystal structure for high iron content, or to a different Fe^{2+}/Fe^{3+} ration between PL2 and PL3.

7. Implications for the Moon

As previously stated, PL is an important constituent of the lunar surface and its presence has been widely recognized through remote sensing. Here, we propose an example of analysis of reflectance spectra acquired from Proclus crater, using the *m3g20090202t024131* image, and we compare lunar spectra with spectra analyzed in Serventi et al. (2013; 2015) and in this paper, underlying why it is important to analyze terrestrial analogues. Proclus crater is 28 km wide, located in the west region of Mare Crisium, where PL (Ohtake et al., 2009; Donaldson Hanna et al., 2011; 2014), PX (Donaldson Hanna et al., 2011) and OL (Donaldson Hanna et al., 2014) were recognized in its crater walls.

Because terrestrial laboratory and lunar M^3 spectra are characterized by a different continuum, due to several factors relate to the different environment conditions, such as space weathering (Gold, 1955), temperature (Burns, 1993), etc., here, we compare spectra after continuum removal.

Fig. 10 shows reflectance spectra from Proclus crater characterized by different spectral properties (the symbols in Fig. 10a represent pixels from which spectra have been acquired). In particular, we can see: a) a spectrum with an absorption band centered at circa 1300 nm and a reflectance

inflection in the 1800 nm region (spectrum "a") and a spectrum with an absorption band centered at circa 1300 nm but without the reflectance inflection in the 1800 nm region (spectrum "b", see dotted lines in Fig. 10b), interpreted as due to Fe^{2+} transition in PL ; b) a spectrum characterized by two absorption bands centered at ca. 950 and 2000 nm, respectively, due to Fe^{2+} transition in PX M2 site (spectrum "c", see grey line in Fig. 10b); and c) a spectrum characterized by a broad absorption band centered at 1050 nm, asymmetric towards the IR region, assigned to Fe^{2+} transition in M1 and M2 sites of OL (spectrum "d", see black line in Fig. 10b).

Spectra "a and b" have been compared with PL1, PL2 and PL3 at three different particle sizes, 36-63 μm, 63-125 μm and 125-250 μm. Fig. 11a shows how spectrum "a" can be compared with PL3 36-63 μm, while in Fig. 11b spectrum "b" is very similar to PL1 36-63 μm. In Fig. 11c spectrum "c" has been plotted with E1 at different particle sizes, while in Fig. 11d spectrum "d" is shown with E4, 36-63 μm, 63-125 μm and 125-250 μm. Lunar and terrestrial spectra in Fig. 11c,d show absorption bands centered at the same wavelengths, with the exception of the coarsest E1; however, in general, lunar spectra are characterized by a very reduced spectral contrast.

Different factors can act to influence the band depth, such as, the mineral chemistry, the absorbing mineral abundance, the number of mineral phases, the particle size, the temperature conditions, the space weathering, etc. . In particular, it is known (Gold, 1995) that the lunar surface is affected by the space weathering: space weathering, on the Moon surface, is a process where formation of nanophase iron particles causes (1) the darkening of overall reflectance, (2) the spectral reddening, and (3) the weakening of absorption bands (McCord and Adams, 1973; Fisher and Pieters, 1994). Thus, space weathering it is an important component that could explain the reduced spectral contrast of lunar M^3 spectra with respect to terrestrial analogue spectra, despite analogy in band centers.

Following these considerations, spectrum "c and d" can be interpreted as characteristic of a relative mature area bearing PX and OL. The effects of the space weathering leads to further considerations

about the "a and b" spectra: the band depth is very reduced if compared with coarse, iron-rich PL, but, as for the previous spectra, this can be related to PL rich relative mature area.

In this paper, we have demonstrated how in mixtures with high content of iron-poor PL the 1250 nm band is almost undetectable when mixed with PX and OL-bearing end-members, thus causing a reduction of the spectral contrast (see Fig. 1a, 2a). In Figs. 11c,d, the spectra from Proclus crater have been compared with ≥90% PL-bearing mixtures.

Fig. 11 generally shows how the interpretation of lunar spectra is not unique; both the space weathering and the mixing with high content of less-absorbing materials can explain spectra with reduce spectral contrast.

8. Conclusions

The improved technologies of the recent lunar missions, e.g., Selene and Chandrayaan-1, permitted to recognize absorption bands of minerals with very low iron content on the lunar surface, such as PL, always considered a spectroscopically transparent mineral in the VNIR. Anorthositic rocks dominate the lunar upper crust: thus, to recognize and quantify PL on the lunar surface is fundamental to infer hypotheses on the Moon's origin and evolution. FAN rocks are composed with more than 90% PL, and have probably been formed by flotation of PL over a magma ocean (Smith et al., 1970; Wood et al., 1970; Warren, 1985; Brown and Elkins-Tanton, 2009). PAN are regions with more than 98% PL (Ohtake et al. (2009) and have been identified in Tycho, Tsiolkovsky, Orientale, and Jackson craters (Ohtake et al., 2009).

For this reason, in this paper we have analyzed mixtures composed with very high PL content and different mafic minerals and we have demonstrated that:

1) PL, mostly if present in high quantity, can be an important contributor to reflectance spectroscopy also affecting mafic mineral absorption bands (as also demonstrated by Cheek and Pieters, 2014);

2) spectral parameters of the Gaussian describing the PL absorption are controlled not only by PL chemistry (and FeO content in its crystal structure), but also by the even very small concentrations of mafic mineralogy (see Fig. 9);
3) PL absorbs in the 1250 nm spectral region but iron-rich PL also affects the longer wavelengths (1600-1800 nm), as revealed by the depth inversion between OPX band I and band II;
4) PX is easily recognizable in mixtures with PL even for very low PX concentration (~1%);
5) OL, if less than 5%, can be masked by iron-rich PL.

Furthermore, laboratory data have been applied to real, lunar cases, revealing the advantages and the limits about studying terrestrial analogues for the mineralogical interpretation of planetary surfaces. Here, for example, we have demonstrated how the possible distinction between FAN and PAN (PL>98%, Othake et al., 2009) depends on the mafic assemblage with which PL is mixed: the distinction is possible in OPX and OPX+CPX- mixtures, while it is difficult in OL-mixtures, where the mafic limit move to 3-4% in mixtures with iron-rich PL.

Spectra in Fig. 10,11 point out why it is important to analyze terrestrial analogues to obtain information about the mineralogy and the particle size of a planetary surface, e.g. to distinguish between iron-poor and iron-rich PL (Fig. 11a,b). On the other hand, Fig. 11c,d show how relating the spectral parameters to the mineralogical composition could not always be a simple task, due to the spectral convergence of different mineralogical compositions, such as mature PX/OL with reduced spectral contrast and mixtures composed with high percentage of iron-poor PL and PX/OL.

Acknowledgments

Spectroscopic measurements were carried out at Inaf-IAPS-Istituto Nazionale di Astrofisica, Roma. EMPA analyses have been performed at Dipartimento di Geoscienze, Padova. E4 end-member has been kindly provided by Dr. Sabrina Ferrari, Department of Geosciences, University of Padova. Financial support by Agenzia Spaziale Italiana, SIMBIO-SYS project.

The authors are also grateful to Leah Cheek and to an anonymous reviewer for the stimulating comments and useful suggestions.

References

Adams, J. B., McCord, T.B., 1971. Optical properties of mineral separates, glass and anorthositic fragments from Apollo mare samples. Proc. Lunar Sci. Conf. 2nd, 2183-2195.

Adams, J. B., Goulland, L. H., 1978. Plagioclase feldspar: visible and near infrared diffuse reflectance spectra as applied to remote sensing. PLPSC, 3, 2901-2909.

Adams, J. B., Hörz, F., Gibbons, R. V., 1979. Effects of shock-loading on the reflectance spectra of plagioclase, pyroxene and glass. Lunar. Planet. Sci. 10. 1-3.

Bell, P. M., Mao, H. K., 1972. Crystal-field studies of lunar samples. Carnegie Inst. Yearb. 71, 480-489.

Boardman, J. W., et al., 2011. Measuring moonlight: an overview of the spatial properties, lunar coverage, selenolocation, and related level 1B products of the Moon Mineralogy Mapper. J. Geophys. Res., 116, E00G14

Brown, S. M., Elkins-Tanton, L. T., 2009. Composition of Mercury's earliest crust from magma ocean models. Earth Planet. Sci., 286, 446-455.

Burns, R.G., 1993. Mineralogical applications of crystal field theory. Cambridge University Press, Cambridge. 551 pp.

Bussey, D.B.J., Spudis. P.D., 2000. Compositional studies of the Orientale, Humorum, Nectaris, and Crisium lunar basins. J. Geophys. Res 105, 4235–4243.

Carli, C., Ciarniello, M., Capaccioni, F., Serventi, G., Sgavetti, M., 2014. Spectral variability of plagioclase-mafic mixtures (2): investigation of the optical constant and retrieved mineral abundance dependence on particle size distribution. Icarus, 235, 207-219.

Cheek, L. C., Pieters, C.M., Parman, S.W., Dyar, M.D., Speicher, E.A., Cooper, R.F., 2011. Spectral characteristics of PL with variable iron content: application to the remote sensing of the lunar crust. Lunar. Planet. Sci. 42. Abstract 1617.

Cheek, L.C., Pieters, C.M., 2012. Variations in anorthosite purity at Tsiolkovsky crater on the Moon. Lunar. Planet. Sci. 43. Abstract 2624.

Cheek, L. C., Donaldson Hanna, K.L., Pieters, C.M., Head, J.W., Whitten, J.L., 2013. The distribution and mineralogy of anorthosite across the Orientale Basin: new perspective from Moon Mineralogy Mapper data. JGR, 118, 1-16

Cheek, L. C., Pieters, C. M., 2014. Reflectance spectroscopy of plagioclase-dominated mineral mixtures: implication for characterizing lunar anorthosites remotely. Am. Min., 99, 1871-1892.

Clark, R.N., Roush, T.L., 1984. Reflectance Spectroscopy: Quantitative Analysis Techniques for Remote Sensing Applications. J. Geophys. Res. 89, 6329-6340.

Clenet, H., et al., 2011. A new systematic approach using the Modified Gaussian Model: insight for the characterization of chemical composition of olivines, pyroxenes and olivine-pyroxene mixtures. Icarus, 213, 404-422

Cloutis, E.A., Gaffey, M.J., 1991. Pyroxene spectroscopy revisited: spectral-compositional combinations and relationships to geothermometry. J. Geophys. Res. 96, 22809-22826.

Donaldson Hanna, K. L., et al., 2011. Diviner and Moon Mineralogy Mapper integrated observation of plagioclase-rich regions on the Moon. Lunar. Planet. Sci. 42. Abstract 2504.

Donaldson Hanna, K. L., et al., 2014. Global assessment of pure crystalline plagioclase across the Moon and implications for the evolution of the primary crust. J. Geophys. Res. Planets. 119, doi:10.1002/2013JE004476.

Fischer, E. M., Pieters, C. M., 1994. Remote Determination of Exposure Degree and Iron Concentration of Lunar Soils Using VIS-NIR Spectroscopic Methods. *Icarus*, 111, 475-488, http://doi.org/10.1006/icar.1994.1158

Gold, T., 1955. The lunar surface. Monthly Notice Royal Astron Soc, 115, 585-604

Green, R. O., et al., 2011. The Moon Mineralogy Mapper (M^3) imaging spectrometer for lunar science. Instrument description, calibration, on-orbit measurements, science data calibration and on-orbit validation. J. Geophys. Res., 116, E00G19.

Hapke, B., 2001. Space weathering from Mercury to the asteroid belt. J. Geophys. Res., 106(E5), 10,039-10,073.

Hawke, B.R., et al., 2003. Distribution and modes of occurrence of lunar anorthosite. J. Geophys. Res., Vol. 108, doi:10.1029/2002JE001890.

Heisenger, H., Head, J., W. III, (2006). New views of lunar geosciences: an introduction and overview. Rev. in Mineralogy and Geochemistry, 60, 1-81.

Hiroi, T., Pieters, C. M., 1994. Estimation of grain sizes and mixing ratios of fine powder mixtures of common geologic minerals. J. Geophys. Res., Vol. 99, 10867-10879

Hiroi, T., et al., 2012. Diversity in the visible-NIR absorption band characteristics of lunar and asteroidal plagioclase. Lunar. Planet. Sci. 43. Abstract 1168

Kato , M., Sasaki, K., Tanaka, K., Iijima, Y., Takizawa, Y., 2008. The Japanese lunar mission SELENE: Science goals and present status. Adv. Space Res., 42, 294-300

Klima, R. L., Pieters, C. M., Dyar Darby, M., 2008. Characterization of the 1.2 μm M1 pyroxene band: extracting cooling history from near-IR spectra of pyroxenes and pyroxene-dominated rocks. Met. Planet. Sci., 43, 1591-1604.

Kramer, G. Y., Kring, D. A., Mahm, A. L., Pieters, C. M., 2013. Spectral and photogeologic mapping of Schrödinger Basin and implications for post-South Pole-Aitken impact deep subsurface stratigraphy. Icarus, 223, 131-148

Matsunaga, T., et al., 2008. Discoveries on the lithology of lunar crater central peaks by SELENE Spectral Profiler. Geophys. Res. Let., 35, L23201, doi:10.1029/2008GL035868

McCord, T. B., Adams, J. B., 1973. Progress in remote optical analysis of lunar surface composition. The Moon 7, 453-474

McEwen A. S., Pieters, C. M., 1997. Mapping the Moon by Clementine. Adv. Space Res. 19, 1523-1533

McGee, J. J., 1993. Lunar ferroan anorthosites: mineralogy, compositional variations, and petrogenesis. JGR, 98, 9089-9105

Ogawa, Y., et al., 2011. The widespread occurrence of high-calcium pyroxene in bright-ray craters on the Moon and implications for lunar-crust composition. Geophys. Res. Let. 38, L17202, doi:10.1029/2011GL048569

Ohtake M., et al., 2008. Performance and scientific objectives of the SELENE (KAGUYA) Multiband Imager. Earth, Planets and Space, 60, 257-267

Ohtake, M., et al., 2009. The global distribution of pure anorthosite on the Moon. Nature 461, doi:10.1038/nature08317

Papike, J., L. A. Taylor, and S. Simon (1991), Lunar minerals, in The Lunar Sourcebook, edited by G. Heiken, D. Vaniman, and B. French, pp. 121 – 181, Cambridge Univ. Press, New York.

Pieters, C. M., Fischer, E. M., Rode, O., Basu, A., 1993. Optical effects of space weathering: the role of the finest fraction. J. Geophys. Res., 98, 20,817-20,824.

Pieters, C. M., 1996. Plagioclase and maskelynite diagnostic features. Lunar. Planet. Sci. 27, Abstract 1031

Pieters, C. M., et al., 2009. The Moon Mineralogy Mapper (M^3) on Chandrayaan-1. Current Science, 96, 500-505

Pieters, C. M., 2000. Space weathering on airless body: resolving a mystery with lunar samples. Meteorit. Planet,. Sci., 35, 1101-1107.

Serventi, G., Carli, C., Sgavetti, M., Ciarniello, M., Capaccioni, F., Pedrazzi, G., 2013. Spectral variability of plagioclase-mafic mixtures (1): effects of chemistry and modal abundance in reflectance spectra of rocks and mineral mixtures. Icarus, 226, 282-298.

Serventi, G., Carli, C., Sgavetti, M., 2015. Spectral variability of plagioclase-mafic mixtures (3): quantitatively analysis applying the MGM algorithm. Icarus, 254, 34-55 doi:10.1016/j.icarus.2015.03.024

Smith, J. V., et al., 1970. Petrologic history of the Moon inferred from petrography, mineralogy, and petrogenesis of Apollo 11 rocks. Proceedings of the Apollo 11 Lunar Sci. Conf., 1, 897-925.

Spudis, P.D., Hawke, B.R:, Lucey, P.G., 1984. Composition of Orientale Basin Deposits and Implications for the Lunar Basin-Forming Process. J. Geophys. Res., Vol. 89, 197-210

Sunshine, J.M., et al., 1990. Deconvolution of mineral absorption bands: an improved approach. J. Geophys. Res., Vol. 95, 6955-6966.

Sunshine, J.M., Pieters, C. M., 1993. Estimating modal abundances from the spectra of natural and laboratory pyroxene mixtures using the Modified Gaussian Model. J. Geophys. Res., Vol. 98, 9075-9087.

Sunshine, J.M., Pieters, C. M., 1998. Determining the composition of olivine from reflectance spectroscopy. J. Geophys. Res., Vol. 103, 13675-13688.

Taylor, A.T., et al., 2009. Lunar magma ocean crust: implication of FeO contents in plagioclase. Lunar. Planet. Sci. 40. Abstract 1304.

Tompkins, S., Pieters, C. M., 1999. Mienralogy of the lunar crust: results from Clementine. Meteoritics & Planetary Science, 34, 25-41.

Warren, P.H., 1985. The magma ocean concept and lunar evolution. Annu. Rev. Earth Planet. Sci., 13, 201-240.

Wood, J.A., Dickey, J.S:, Marvin, U.B., and Powell, B.N., 1970. Lunar anorthosites and a geophysical model of the Moon. Proc. Apollo 11 Lunar Sci. Conf., 965-988.

Yamamoto, S., et al., 2010. Possible mantle origin of olivine around lunar impact basins detected by SELENE. Nature, 3, DOI: 10.1038/NGEO897

Figure captions

Fig. 1 Reflectance spectra at the 36-63 μm particle size. a)E5+PL1; b)E5+PL2; c)E5+PL3; d)E1+PL1; e)E1+PL2; f)E1+PL3; g)E4+PL1; h)E4+PL2; i)E4+PL3. Plagioclase modal abundance increases from the bottom (dashed line spectrum) to the top (black spectrum).

Fig. 2 Reflectance spectra at the 36-63 μm particle size after continuum-removal. a)E5+PL1; b)E5+PL2; c)E5+PL3; d)E1+PL1; e)E1+PL2; f)E1+PL3; g)E4+PL1; h)E4+PL2; i)E4+PL3. Plagioclase modal abundance increases from the bottom (dashed line spectrum) to the top (black spectrum).

Fig. 3 MGM deconvolution and residuals of mafic end-members (a,b,c) and plagioclases (d,e,f). a) E5 end-member is deconvolved with 3Gaussians, 2 in the 800-1000 nm range, G1 for Fe^{2+} in OPX and G5 for adjustment (for further explanation refer to the text), and in the NIR range G3 for Fe^{2+} in OPX; b) E1 end-member is decomposed with 5 Gaussians, 3 in the 800-1000 nm range, G1 for Fe^{2+} in OPX, G2 for Fe^{2+} in CPX and G5 for adjustment, and 2 in the NIR range, G3 for Fe^{2+} in OPX and G4 for Fe^{2+} in CPX; c) E4 end-member is decomposed with 3 Gaussians, G6, G7 and G8, due to Fe^{2+} transition in M1 and M2 sites of OL; d) PL1 is decomposed with G10 centered at ca. 1200-1250 nm for the Fe^{2+} in PL, and G11 in the 1600-1800 nm spectral region and other Gaussian for the vibrational bands due to OH alteration; e) PL2 is decomposed with G10 centered at ca. 1200-1250 nm for the Fe^{2+} in PL, G11 at ca. 1800 nm; f) PL3 is decomposed with G10 centered at ca. 1200-1250 nm for the Fe^{2+} in PL, G11 at ca. 1800 nm. Gaussians describing the vibrational bands due to OH alteration are not described in the text and in the discussions.
The residuals of the mafic end-members and PL1 are generally between ±0.05. However, considering PL2 (Fig. 3e) and PL3 (Fig. 3f), the residuals show a sinusoidal pattern in the 1000-1500 nm spectral region that could indicate the lacking of a Gaussian. We preferred to explain this

behavior with a possible asymmetry or saturation effects of the PL band, also considering the reflectance decrease in the 1600-1800 nm spectral region, thus not adding further Gaussians.

Fig. 4 The figure shows the spectral parameter variations in mixtures composed with E5 and PL. In particular, with increasing PL content: a,b) c0 and, above all, c1, become less negative; c) the PL band depth deepens (with PL2 deeper than PL3); d) PL center does not show significant variations, even if 98% and 99% PL3-bearing mixture center are shifted towards longer wavelengths with respect to the other PL3-bearing mixtures; e) PL band width is almost unchanged in PL2 and PL3 mixtures while it widens in PL1-mixtures.
B.C. : band center; B.D. : band depth; B.W.: band width.

Fig. 5 The figure shows the band depth variation in mixtures composed with E5 and PL. a) PL and mafic mineral depths; while PL deepens, mafic band depth decrease. In particular, PL1 band dominates only for more than 99% PL, while PL2 and PL3 bands are the deepest from 95% PL. a1-a3) Enlargement of Fig. 5a: for PL1, PL2<98% and PL3< 96%, OPX band I is deeper than OPX Band II, while for PL2≥ 98% and PL3≥ 96% there is an overturn and the OPX band II become deeper (see squares).

Fig. 6 The figure shows the spectral parameter variations in mixtures composed with E1 and PL. In particular, with increasing PL content: a,b) c0 and, above all, c1, become less negative; c) the PL band depth deepens (with PL2 slightly deeper than PL3); d) PL center does not show significant variations; f) PL band width is almost unchanged, while in PL1-mixtures PL band widens.
B.C. : band center; B.D. : band depth; B.W.: band width.

Fig. 7 The figure shows the band depth variation in mixtures composed with E1 and PL. a) PL and mafic mineral depths; while PL deepens, mafic band depth decrease. In particular, PL1 band

dominates for more than 97% PL, while PL2 and PL3 bands are the deepest from 92% PL. a1-a3) Enlargement of Fig. 5a: for PL1, PL2<97% and PL3< 92%, OPX band I is deeper than OPX Band II, while for PL2>97% and PL3> 92% there is an overturn and the OPX band II become deeper (see squares).

Fig. 8 The figure shows the spectral parameter variations in mixtures composed with E4 and PL. In particular, with increasing PL content: a,b) c0 is almost unaffected, while c1 becomes less negative; c) COMP band becomes less deep but is always deeper than OL band 1 and 2; d) COMP band center moves towards the IR region; e) COMP band width is slightly narrow; f) 1800 nm band deepens; g) 1800 nm band moves towards shorter wavelengths; h) 1800 nm band widens.
B.C. : band center; B.D. : band depth; B.W.: band width.

Fig. 9 The figure shows the comparison between all the mixtures analyzed in this paper. a) PL band depth decreases in OL-mixtures, while it deepens in PX-mixtures; in general, PL band is deeper in E5-mixtures with respect to E1-mixtures, and PL2 band is deeper than PL3 band; b) COMP band is centered at shorter wavelength in OL-mixtures with respect to the PL band center in PX-mixtures. In PX-mixtures: 1) in PL1-bearing mixtures, OPX+CPX-mixtures are at longer wavelength than OPX-mixtures; 2) in PL2-bearing mixtures, OPX+CPX-mixtures and OPX-mixtures are at similar wavelength; and 3) in PL3-bearing mixtures, OPX-mixtures are at longer wavelength than OPX+CPX-mixtures; c) PL band width only slightly varies, with the exception of PL1 in E1 and E5-mixtures where PL band substantially widens.
B.C. : band center; B.D. : band depth; B.W.: band width.

Fig. 10 a) Proclus crater as mapped by M^3 (image *m3g20090202t02413*), yellow symbols represents pixel from which spectra were acquired; b) continuum-removed spectra of three different mineralogies from Proclus crater. In particular: spectrum “a” (black, dotted line in Fig.) shows an

absorption band centered at circa 1300 nm and a reflectance decrease in the 1800 nm region, interpreted as due to Fe^{2+} transition in PL; spectrum "b" (black, narrow-dotted line in Fig.) with an absorption band centered at circa 1300 nm, interpreted as due to Fe^{2+} transition in PL; spectrum "c" (grey line in Fig.) characterized by two absorption bands centered at 980 and 1980 nm, respectively, due to Fe^{2+} transition in PX M2 site; and spectrum "d" (black line in Fig.) characterized by a broad absorption band centered at 1020 nm, asymmetric towards the IR region, assigned to Fe^{2+} transition in M1 and M2 sites of OL.

Fig. 11 Comparison between lunar spectra and terrestrial analogues analyzed in this paper and in Serventi et al. (2013; 2015). a) spectrum "a" has been plotted with PL1, PL2 and PL3 at three different particle sizes, 36-63, 63-125 and 125-250 μm; spectrum "a" can be compared with PL3, 36-63 μm; b) spectrum "b" has been plotted with PL1, PL2 and PL3 at three different particle sizes, 36-63, 63-125 and 125-250 μm; spectrum "b" can be compared with PL1, 36-63 μm; c) spectrum "c" has been plotted with E1 at three different particle sizes, 36-63, 63-125 and 125-250 μm, and with two mixtures, 90% PL1-E1 and 92% PL1-E1 36-63μm, respectively. Spectrum "c" shows two absorption bands centered at the same wavelengths of E1 but with a reduce depth; on the other hand, spectrum "c" can be compared also with the 92% PL1 mixture; d) spectrum "d" has been plotted with E4 at three different particle sizes, 36-63, 63-125 and 125-250 μm, and with two mixtures, 90% PL1-E4 36-63μm and 92% PL1-E4 63-125μm, respectively. Spectrum "d" shows a broad absorption band centered at the same wavelength of E4 but with a reduced depth; on the other hand, spectrum "d" can be compared also with the 90% PL1 mixture.

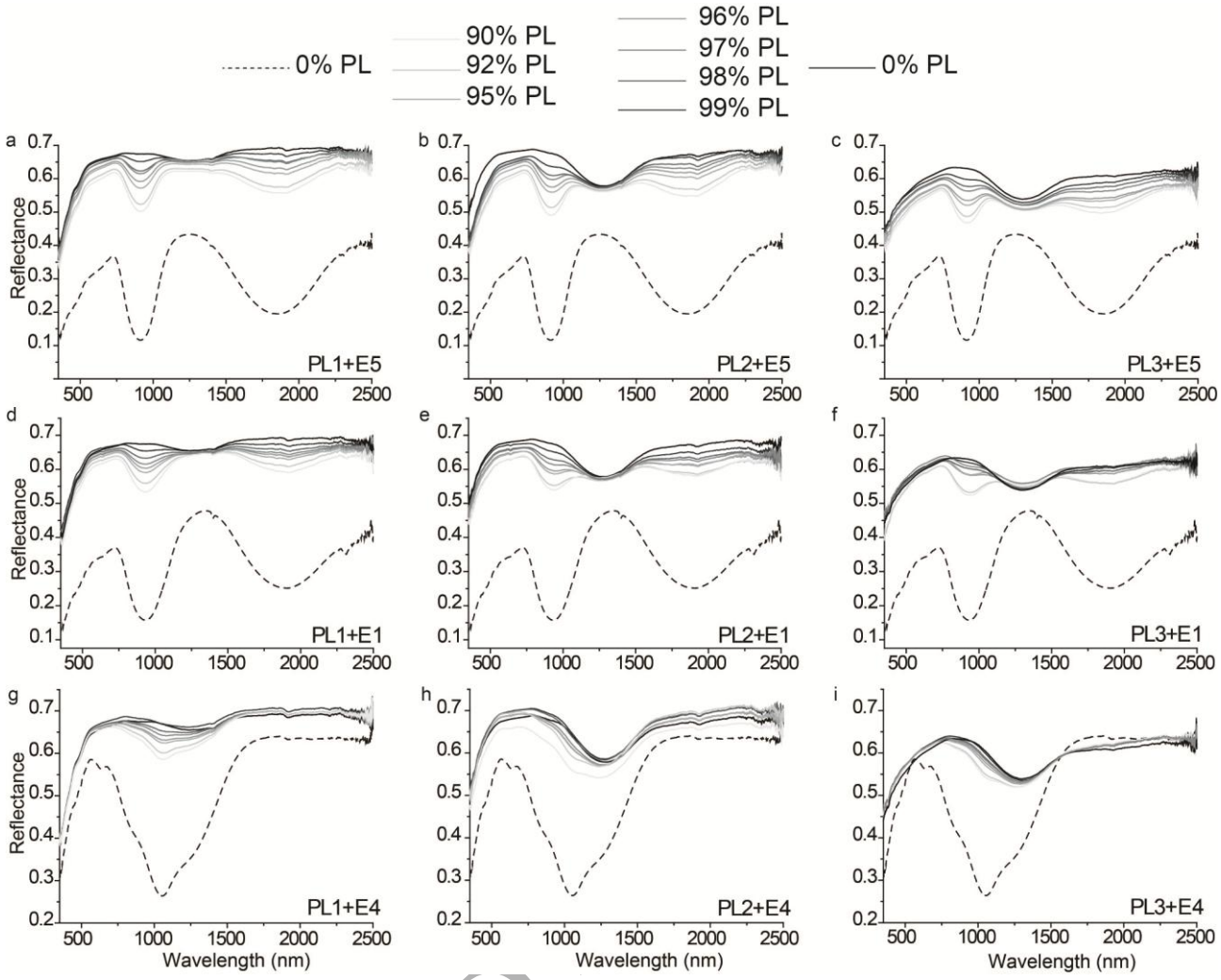

Fig. 1

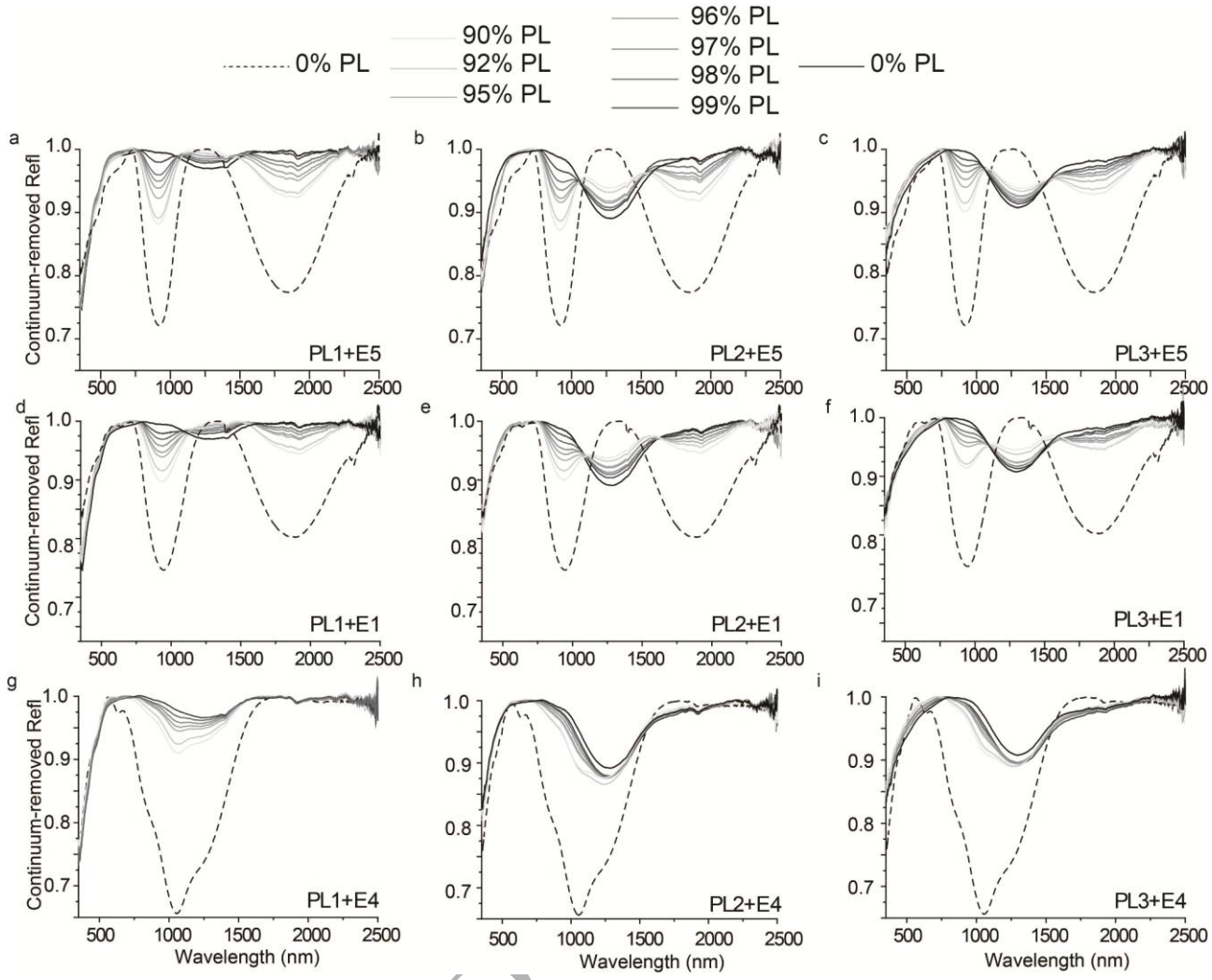

Fig. 2

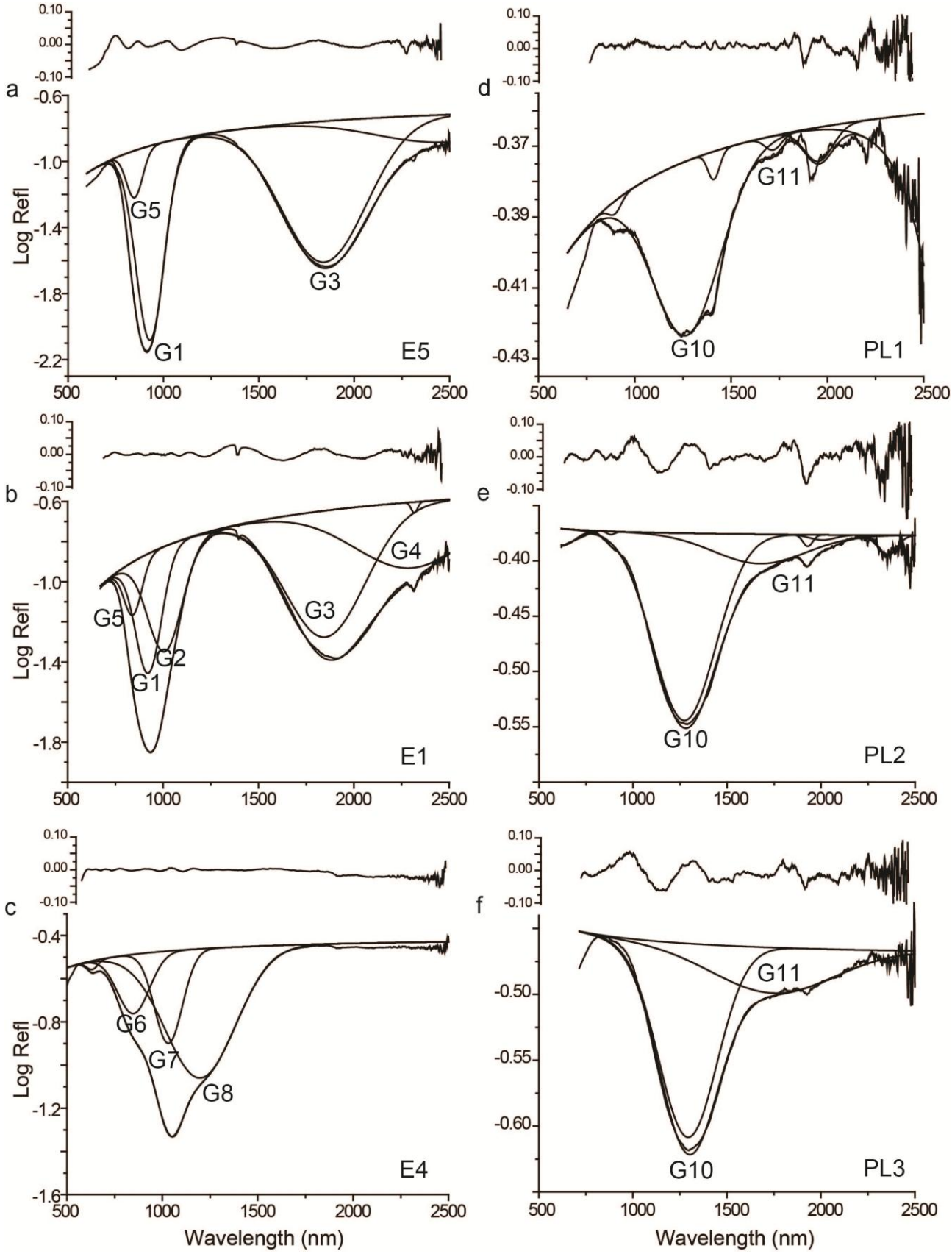
a
G5
G3
G1
E5
b
G4
G5
G3
G2
G1
E1
c
G6
G7
G8
E4
d
G11
G10
PL1
e
G11
G10
PL2
f
G11
G10
PL3
Log Refl
Wavelength (nm)

Fig. 3

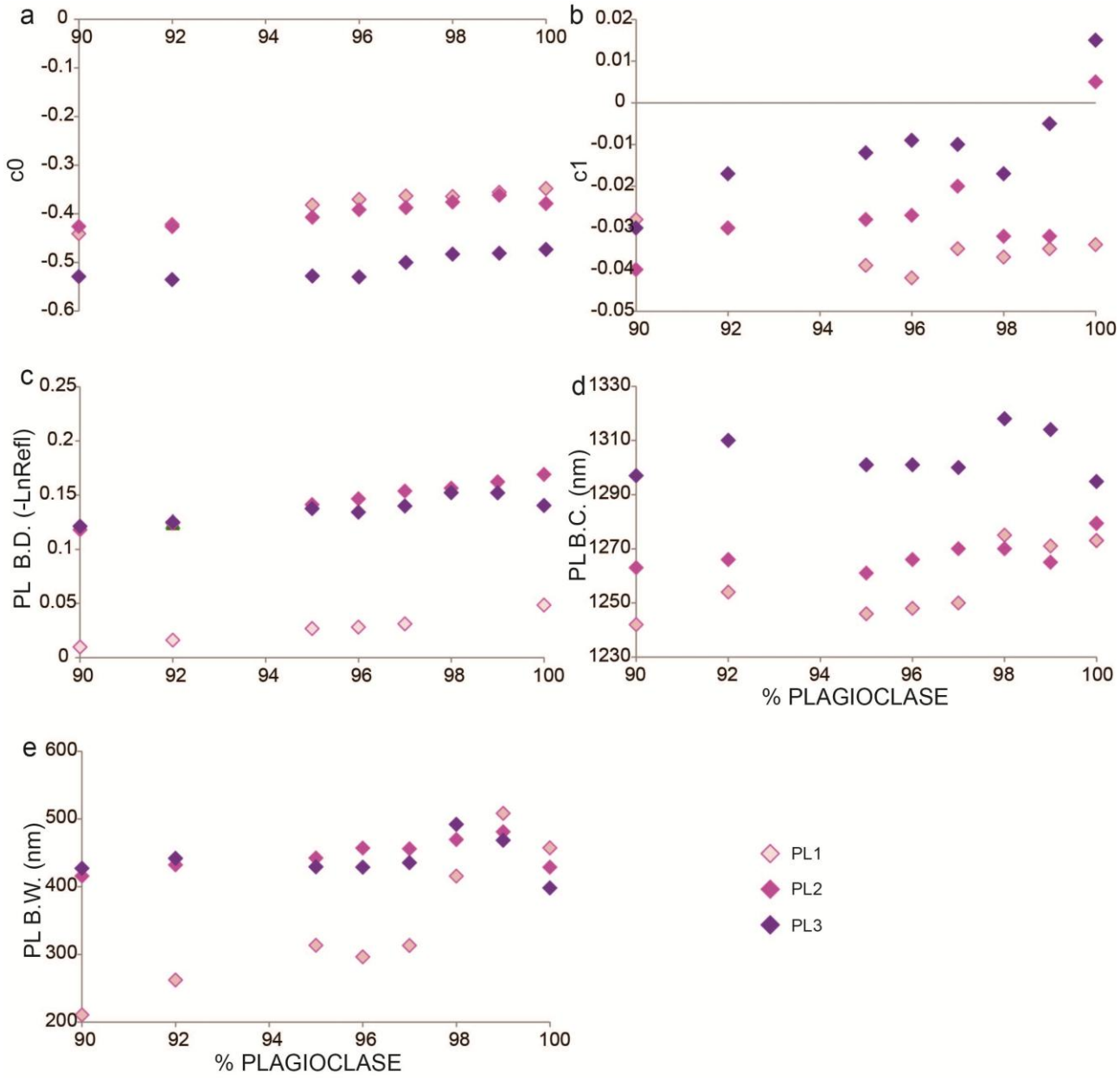

Fig. 4

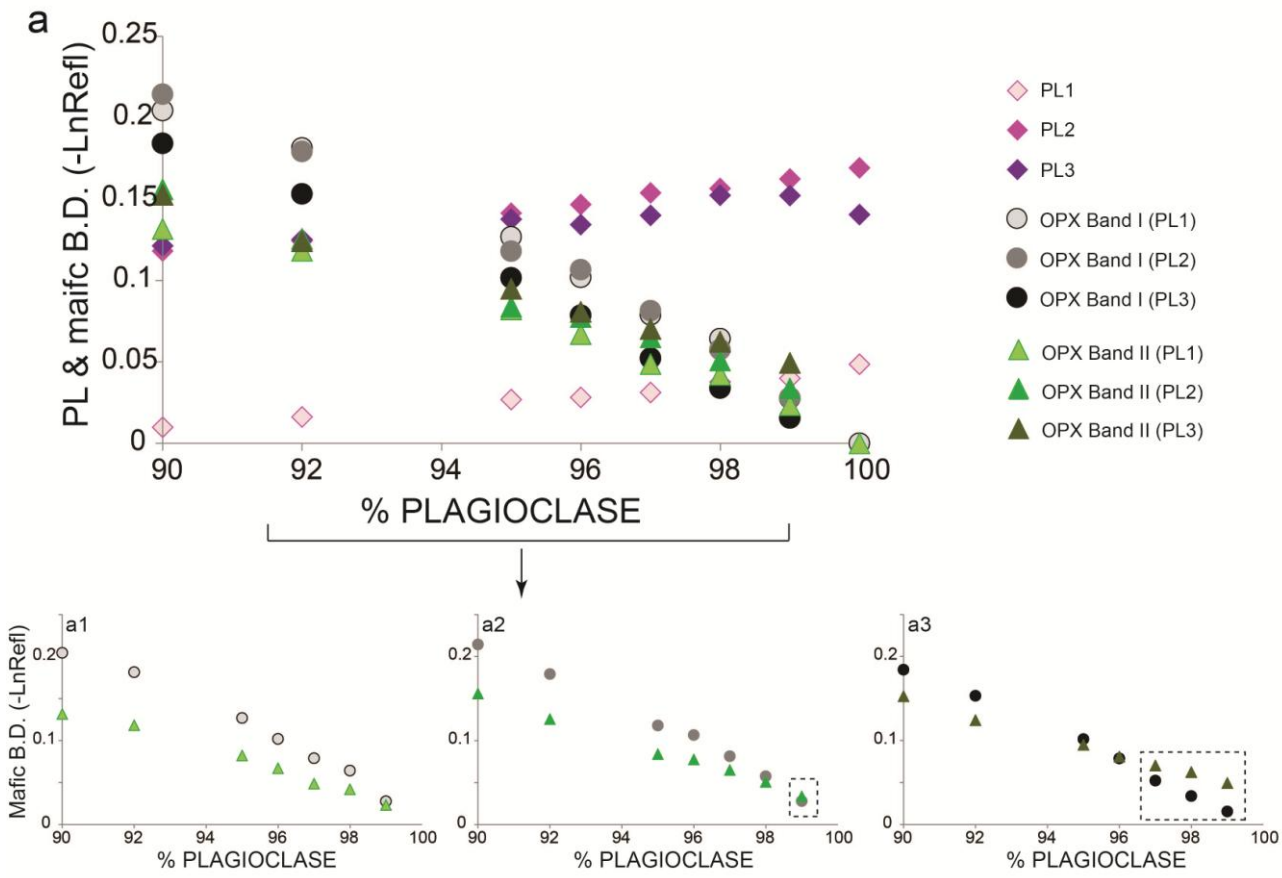

Fig. 5

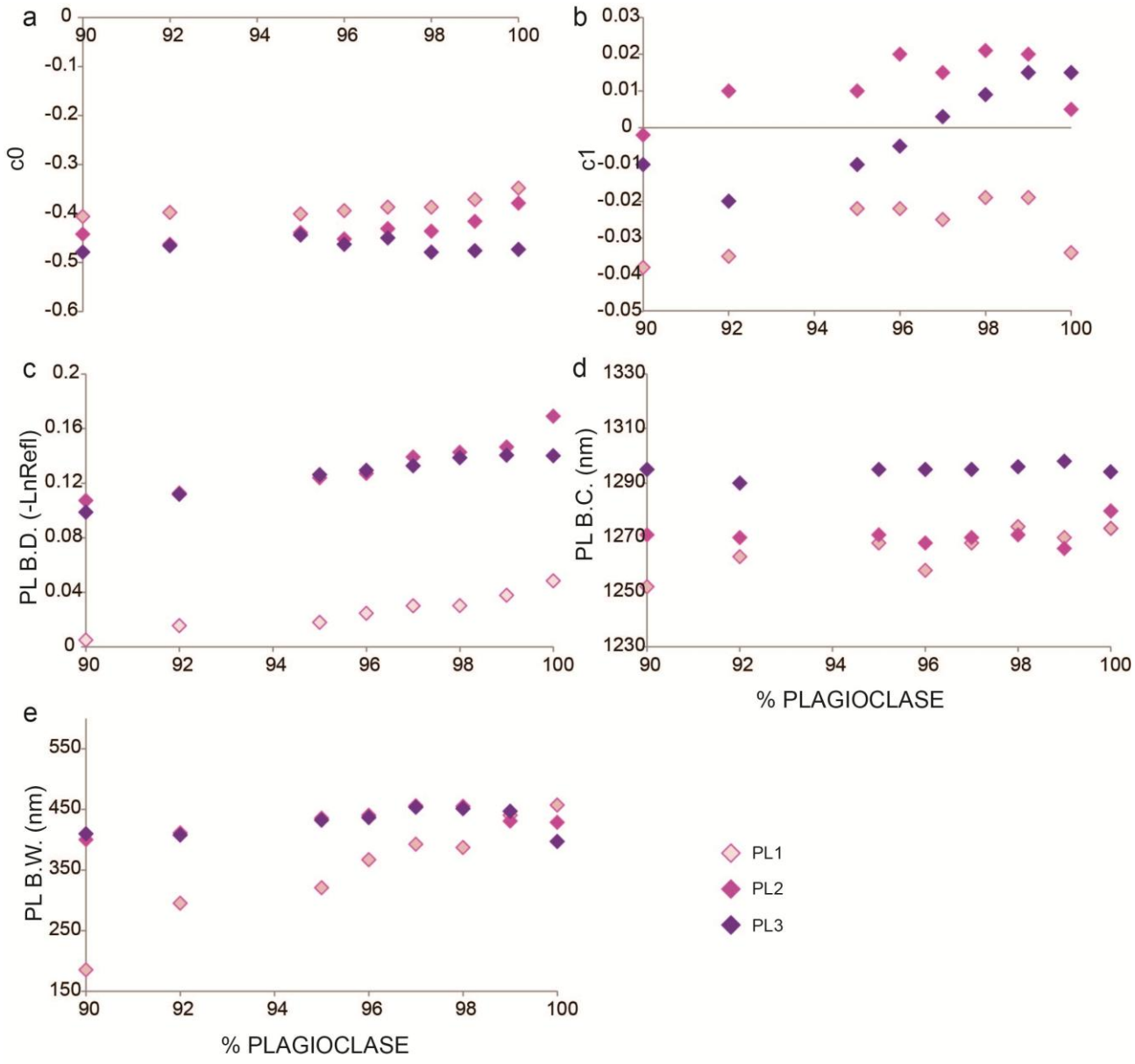

Fig. 6

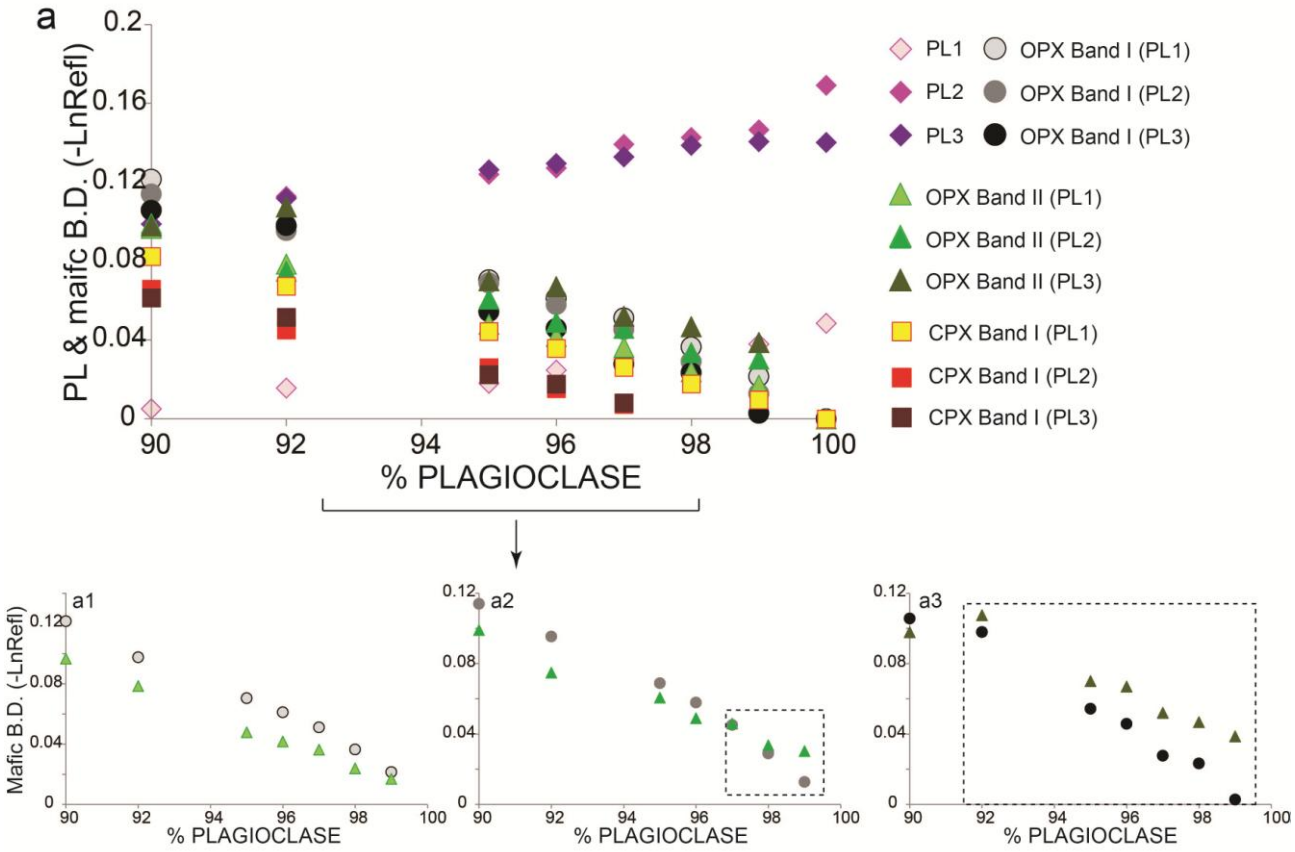

Fig. 7

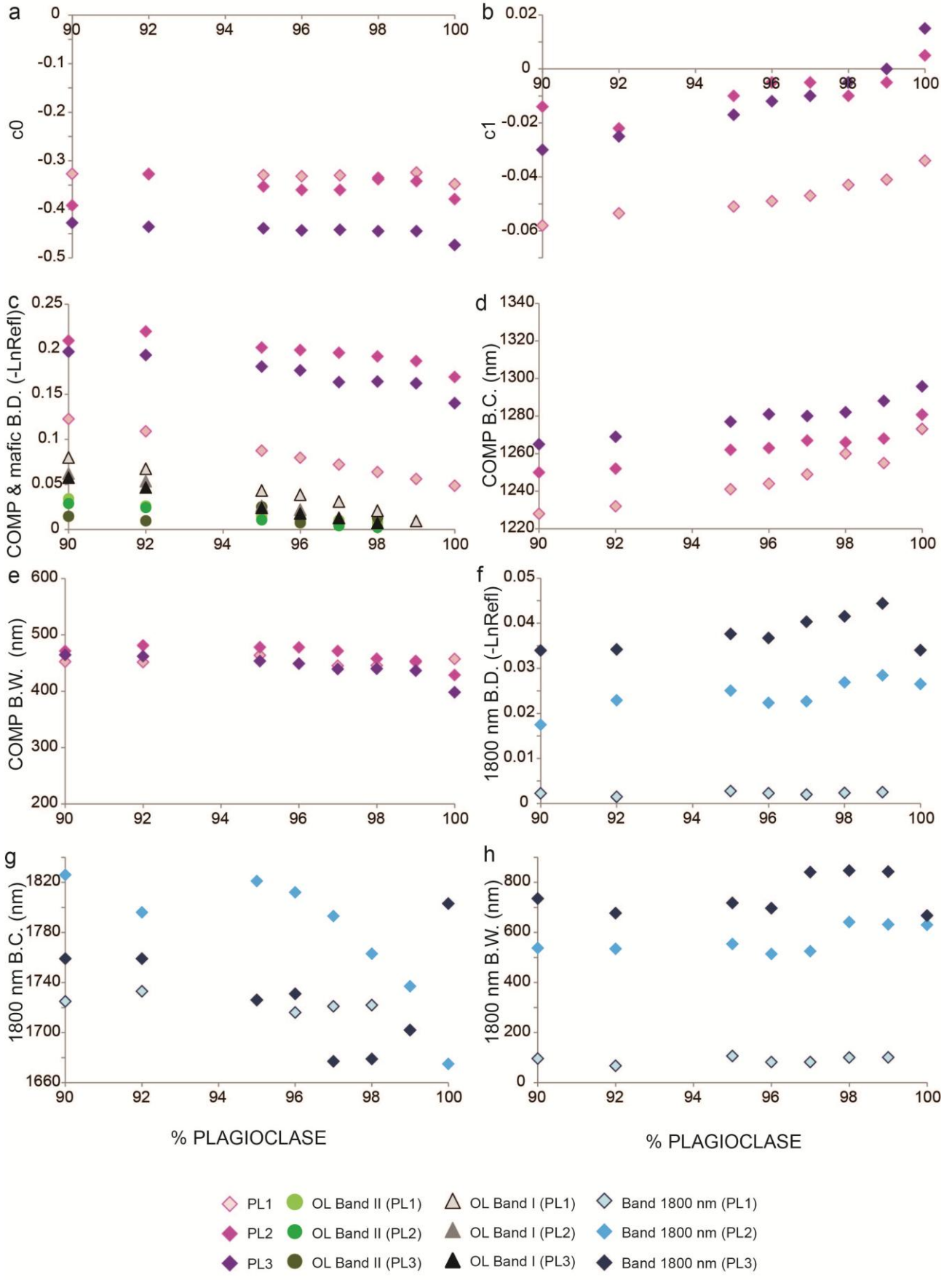
a
c0
b
c1
c
COMP & mafic B.D. (-LnRefl)
d
COMP B.C. (nm)
e
COMP B.W. (nm)
f
1800 nm B.D. (-LnRefl)
g
1800 nm B.C. (nm)
h
1800 nm B.W. (nm)
% PLAGIOCLASE
% PLAGIOCLASE
PL1
PL2
PL3
OL Band II (PL1)
OL Band II (PL2)
OL Band II (PL3)
OL Band I (PL1)
OL Band I (PL2)
OL Band I (PL3)
Band 1800 nm (PL1)
Band 1800 nm (PL2)
Band 1800 nm (PL3)

Fig. 8

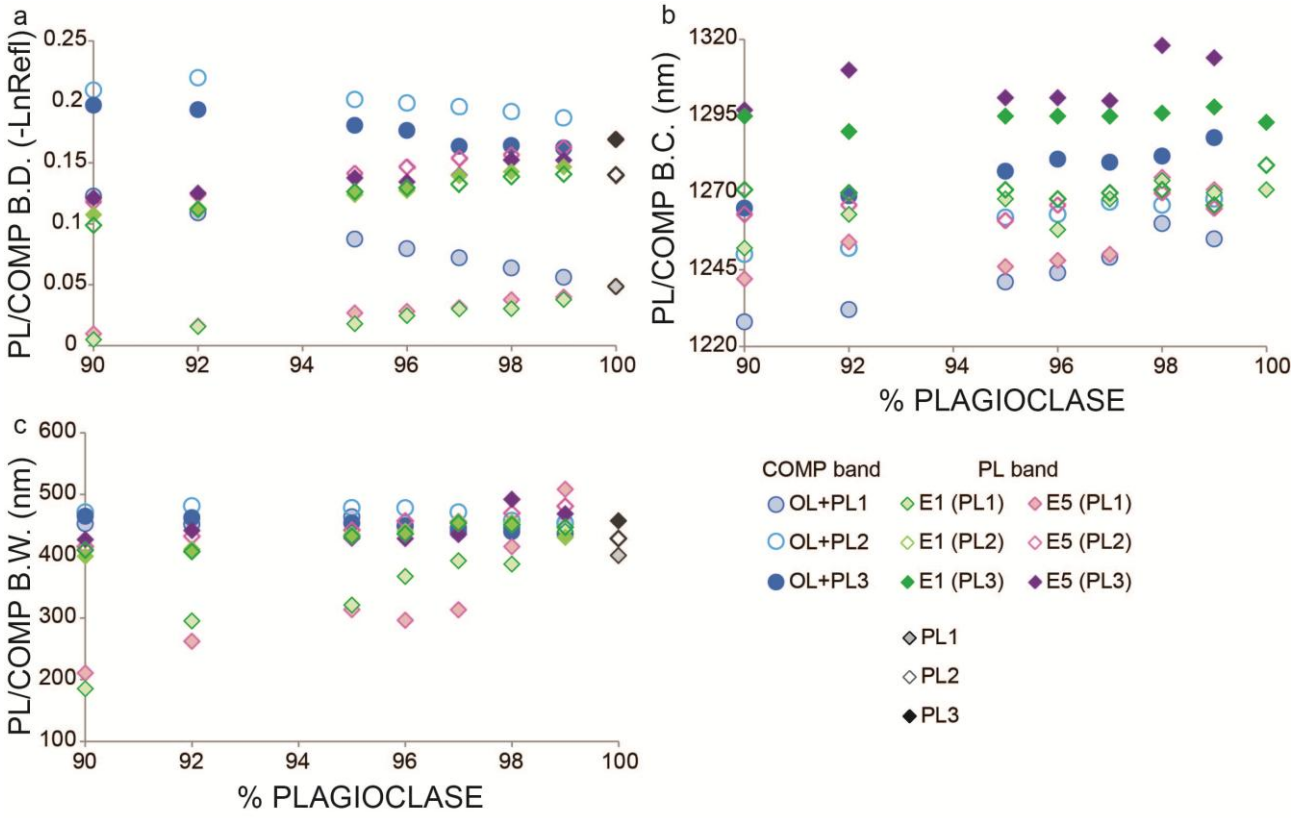
a
PL/COMP B.D. (-LnRefl)
0.25
0.2
0.15
0.1
0.05
0
90
92
94
96
98
100
b
PL/COMP B.C. (nm)
1320
1295
1270
1245
1220
% PLAGIOCLASE
c
PL/COMP B.W. (nm)
600
500
400
300
200
100
% PLAGIOCLASE
COMP band
PL band
OL+PL1
OL+PL2
OL+PL3
E1 (PL1)
E1 (PL2)
E1 (PL3)
E5 (PL1)
E5 (PL2)
E5 (PL3)
PL1
PL2
PL3

Fig. 9

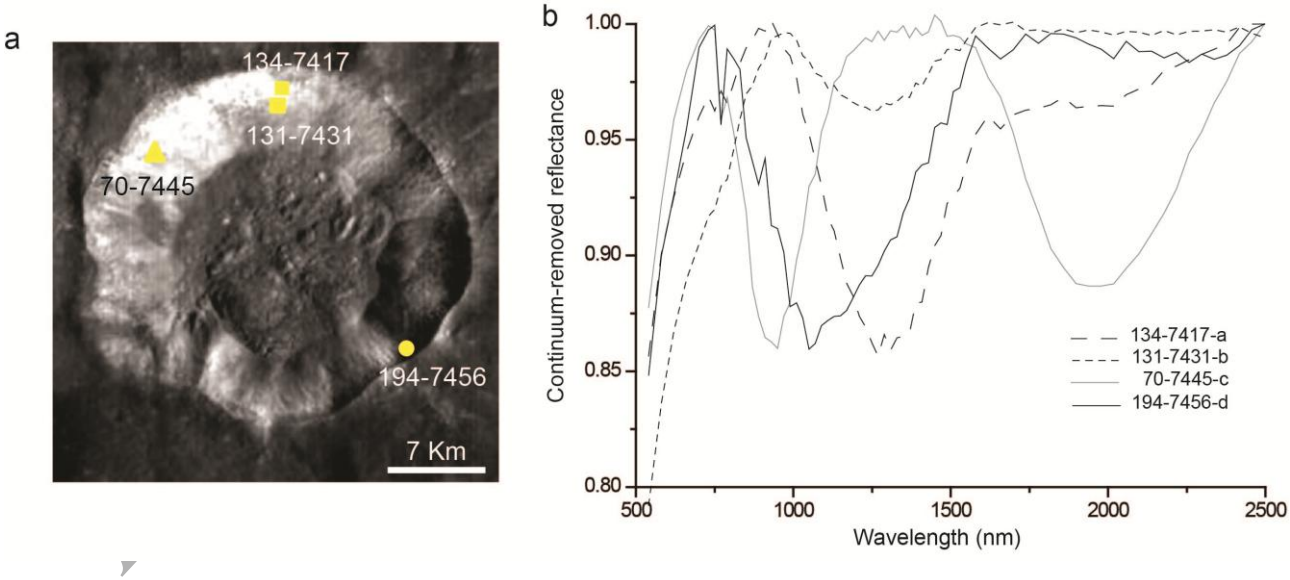
a
134-7417
131-7431
70-7445
194-7456
7 Km
b
Continuum-removed reflectance
1.00
0.95
0.90
0.85
0.80
500
1000
1500
2000
2500
Wavelength (nm)
134-7417-a
131-7431-b
70-7445-c
194-7456-d

Fig. 10

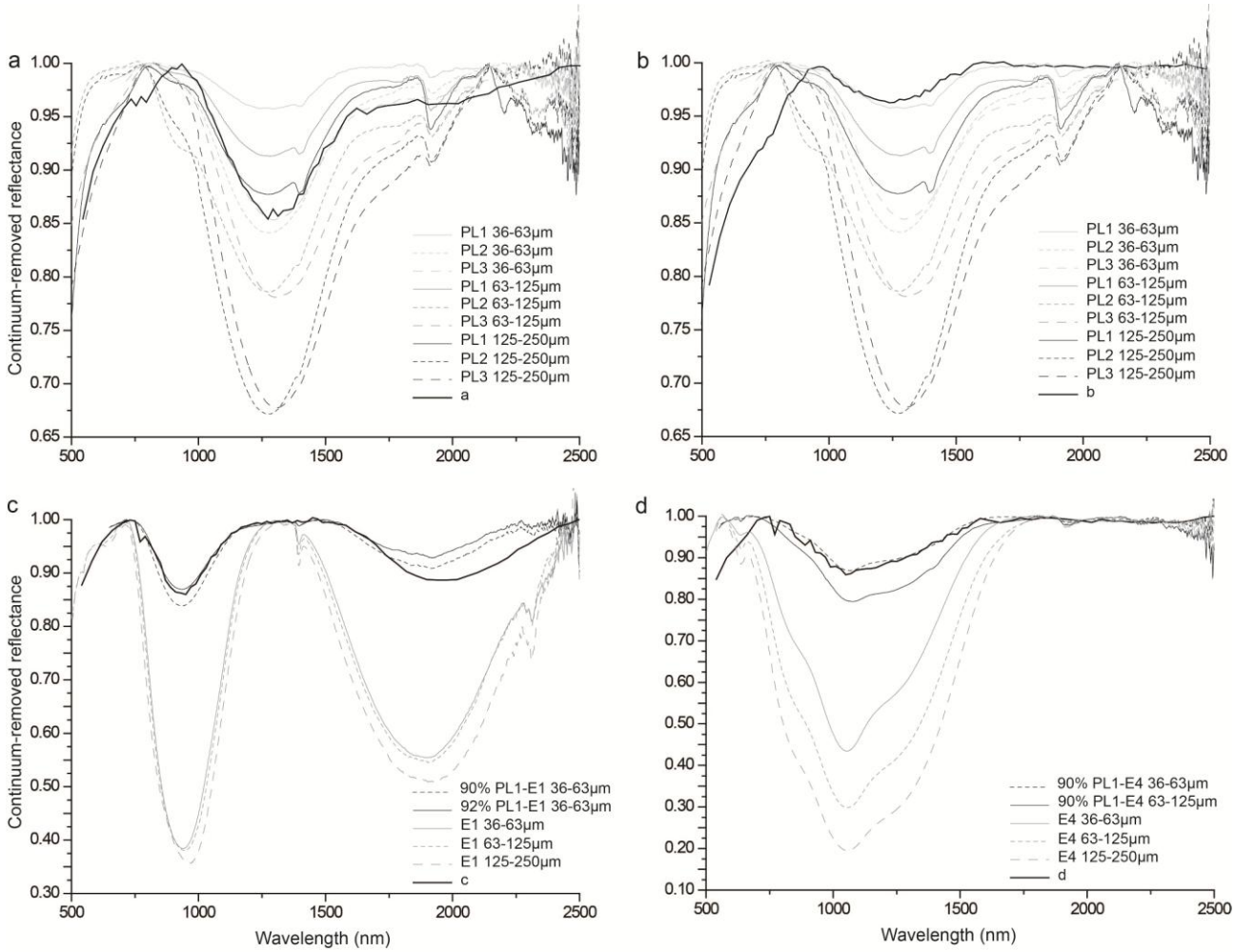

Fig. 11

End-members	Minerals % and Chemistry	FeO wt.% in minerals	Geological setting
E5	OPX(100%) En_{82}	10.67	Stillwater complex
E1	CPX(43.9%) En_{45}-Wo_{46}	5.72	Stillwater complex
	OPX(56.1%) En_{77}	13.45	
E4	OL(100%) Fo_{90}	9.73	Arizona
PL1	An_{45}	0.1	Bjerkreim Sokndal
PL2	An_{80}	0.36	Stillwater complex
PL3	An_{80}	0.5	Stillwater complex

Tab.1 Table shows the end-member's chemistry, the relative FeO wt.% content in each mineral and the geological setting.

Gaussian	Position (nm)	Interpretation
G1	900-950	Fe^{2+} in OPX M2 site
G2	1000-1100	Fe^{2+} in CPX M2 site
G3	1850	Fe^{2+} in OPX M2 site
G4	2300	Fe^{2+} in CPX M2 site
G5	840	Adjustment Gaussian
G6	850-950	Fe^{2+} in OL M1 site
G7	1000-1100	Fe^{2+} in OL M2 site
G8	1200-1250	Fe^{2+} in OL M1 site
G10	1250-1300	Fe^{2+} in PL
G11	1600-1800	PL asymmetry

Tab. 2 In the table are reported a list of Gaussians used in the end-member deconvolution, the wavelength position and the mineralogical interpretation.

	E1		
	Center	Width	Depth
G5	842	120	-0.2645
G1	924	174	-0.5967
G2	1010	233	-0.5252
G3	1851	539	-0.6309
G4	2305	784	-0.3042

	E4		
	Center	Width	Depth
G6	848	215	-0.2743
G7	1032	188	-0.4274
G8	1199	475	-0.5983

	E5		
	Center	Width	Depth
G5	848	110	-0.2848
G1	930	191	-1.176
G3	1843	575	-0.8535

Tab. 3 In table are reported the spectral parameters obtained by MGM deconvolution of mafic end-members, at the 36-63 μm. Center and width are expressed in nanometers, while depth as the logarithm of the reflectance.

	PL1		
	Center	Width	Depth
G10	1271	457	-0.0484
G11	1719	168	-0.0039

	PL2		
	Center	Width	Depth
G10	1279	428	-0.1691
G11	1675	630	-0.0266

	PL3		
	Center	Width	Depth
G10	1293	401	-0.1401
G11	1748	830	-0.0346

Tab. 4 In table are reported the spectral parameters obtained by MGM deconvolution of PL, at the 36-63 µm. Center and width are expressed in nanometers, while depth as the negative logarithm of the reflectance.